Design and Calculations of a Broadband Two Color Inline Interferometer

Author:
Neven Ibrakovic

Supervisor:
Johan Mauritsson

Assistant Supervisor:
Esben Witting Larsen

January 21, 2014

High-Order Harmonic generation (HHG) is an alternative and much more compact way of generating x-ray radiation compared to producing it in a synchrotron. In this report a two color inline interferometer is designed to superimpose electrical fields generated by a frequency doubling crystal, for the purpose of reshaping the pulse train generated in the HHG process. The challenges of this design is that the light is composed of very short pulses, hence the light is very broadband. As the light is broadband the interferometer must to some extent be achromatic enough to treat two separate wavelength regimes chromatically whilst treating the entire broadband span of these pulses achromatically. Another challenge is that the interferometer should be constructed so that the temporal offset of the two pulses should be tunable with sub cycle precision. The interferometer has been assembled but only partially tested.

Table of contents

Abbrevations

1. **BBO** Beta-Barium Borate.
2. **SH(G)** Second Harmonic (Generation).
3. **HHG** High-order Harmonic Generation
4. **FS** Fused Silica
5. **XUV** Extreme Ultra Violet radiation

1 Introduction

High-order Harmonic generation (HHG) is one of the most popular disciplines in today's atomic physics as it provides the possibility to produce integer frequencies of a fundamental laser beam with the addition of XUV pulses with attosecond duration. With this one can construct a pulse train of very short pulses having excellent temporal resolution for studying movements on an atomic scale [1]. HHG can conceptionally be understood using a semiclassical three step model. First the atom is ionized by an intense laser field, after ionization the electron is driven by the combined field of the laser and the ion. Under certain circumstances the electron may be driven back to it's parent ion, where it can scatter, recombine, knock out another electron, or simply pass. If the electron and the ion recombine an XUV photon with the excess energy is emitted. The emission of this a XUV photon is what is known as HHG [2]. If the **E**-field has elliptical polarization, it is more probable that the electron will miss the atom and not recombine. This report focuses on a setup that provides the possibility to superimpose two electric fields and thus control the pulse train. When the two fields are superimposed the peak amplitude of the generated driving field is modulated. By tuning the delay between the fields it is possible to increase the amplitude in one part of the light cycle and decrease it in another part, thereby having the ionization step of the HHG only once per cycle instead of twice. This is easiest if the frequency of the wave that is used for modulating has twice the frequency of the fundamental wave. To achieve this a collinear interferometer for frequency doubling was designed. A second harmonic is generated and the fundamental beam is transmitted, the alignment of the polarization is corrected so that both fields are parallel and delay plates are introduced providing sub-cycle delay tunability between the pulses. This device is called an inline two-color interferometer. The collinear setup provides a compact assembly as opposed to having beams separated in two arms and treated individually, but requires more effort in determining suitable optical materials for the assembly. The interferometer is designed for light centred at 1300nm with 300nm wavelength bandwidth. The second harmonic is centred at 650nm and has a 75nm bandwidth. This wavelength region is not standard when conducting experiments of this kind. The bandwidths are very large and contribute to a higher ellipticity than normally when aligning the polarization. The collinear setup is at the moment of writing not fully experimentally tested, and this report treats the theory of creating such an assembly. Given that the interferometer is functional it will mainly be used for generating high-order harmonics, to be used for different kinds of spectroscopy *e.g.* for VMIS (Velocity Mapping Imaging Spectrometer) and/or PEEM (Photo Electron Emission Microscopy).

2 Theory

2.1 Nonlinear media

To produce an overtone, a nonlinear medium is used. Two popular nonlinear media are beta barium borate (BBO) and potassium dihydrogen phosphate (KDP). The application of these crystals in the setup of this report is mainly the Second Harmonic Generation (SHG). In B.E.A Saleh [3] it is stated that the relation between the electric field and polarization for a homogeneous, linear and isotropic medium is denoted by:

$$\mathbf{P} = \varepsilon_0 \chi \mathbf{E}. \tag{1}$$

Since the crystals are not linear media, the susceptibility (χ) may be Taylor expanded around $\mathbf{E} = 0$ in order to obtain the first order nonlinear terms:

$$\mathbf{P} = a_1\mathbf{E} + a_2\frac{1}{2}\mathbf{E^2} + a_3\frac{1}{6}\mathbf{E^3} + ..., \tag{2}$$

with higher orders assumed to be negligible when studying SHG, even the third order term is assumed to be much smaller than the second order term. Convention is to write eq(2) in following form:

$$\mathbf{P} = \epsilon_0\chi^{(1)}\mathbf{E} + 4\epsilon_0 d\mathbf{E^2} + 4\chi^{(3)}\mathbf{E^3} + ..., \tag{3}$$

where $d = \frac{1}{4}a_2$ and $\chi^{(3)} = \frac{1}{24}a_3$ which provide a measure of the strength of the second and third order nonlinear effects. It is convenient to address the nonlinear effects as $\mathbf{P^{NL}}$ so that:

$$\mathbf{P^{NL}} = 4d\epsilon_0\mathbf{E^2} + 4\chi^{(3)}\mathbf{E^3} + ..., \tag{4}$$

which sums the effects of the second and third order nonlinear effects.

2.2 Second harmonic generation

2.2.1 Nonlinear wave equation

Second harmonic generation is a form of sum frequency generation where the sum is composed of two identical frequencies. In order to calculate physical quantities such as electric amplitudes and intensities a wave equation is needed. Since SHG is a nonlinear effect it cannot be described by a linear wave equation and a nonlinear wave equation is needed.
Maxwell's equations in matter are the following:

$$\nabla \cdot \tilde{\mathbf{D}} = \rho, \tag{5}$$

$$\nabla \cdot \tilde{\mathbf{B}} = 0, \tag{6}$$

$$\nabla \times \tilde{\mathbf{E}} = -\frac{d\mathbf{B}}{dt}, \tag{7}$$

$$\nabla \times \tilde{\mathbf{H}} = \frac{d\mathbf{D}}{dt} + \mathbf{j}. \tag{8}$$

The charge density ρ is set to zero since the optical crystals do not have a net charge; this also applies for the free current density $\mathbf{j}$. We chose then to take the curl of eq. (7).

$$\nabla \times (\nabla \times \tilde{\mathbf{E}}) = \nabla \times (-\frac{d\tilde{\mathbf{B}}}{dt}) = -\frac{d}{dt}(\nabla \times \tilde{\mathbf{B}}), \tag{9}$$

$$\tilde{\mathbf{B}} = \mu_0 \tilde{\mathbf{H}} \Rightarrow \nabla \times (\nabla \times \tilde{\mathbf{E}}) = -\frac{d}{dt}(\nabla \times \mu_0 \tilde{\mathbf{H}}) = -\mu_0 \frac{d^2 \tilde{\mathbf{D}}}{dt^2}. \tag{10}$$

Introduced above is the vacuum permeability μ_0, which holds the following relation to the vacuum permittivity, ϵ_0, and the speed of light in vacuum, c,

$$\mu_0 = \frac{1}{\epsilon_0 c^2}. \tag{11}$$

The left term in eq.(9) can be rewritten as:

$$\nabla \times (\nabla \times \tilde{\mathbf{E}}) = \nabla(\nabla \cdot \tilde{\mathbf{E}}) - \nabla^2 \tilde{\mathbf{E}}, \tag{12}$$

where the left term on the right side vanishes, since $\nabla \cdot \tilde{\mathbf{D}}$ is zero and directly proportional to $\nabla \cdot \tilde{\mathbf{E}}$. Using eq. (12) and eq. (11) we can now rewrite eq. (10) as.

$$-\nabla^2 \tilde{\mathbf{E}} = \frac{1}{\epsilon_0 c^2} \frac{d^2 \tilde{\mathbf{D}}}{dt^2}. \tag{13}$$

We now choose to split up the displacement field $\tilde{\mathbf{D}}$ into a linear part and a nonlinear part,

$$\tilde{\mathbf{D}} = \tilde{\mathbf{D}}^{(1)} + \tilde{\mathbf{P}}^{\mathbf{NL}} = \epsilon_0 \epsilon_r(\omega) \tilde{\mathbf{E}} + \tilde{\mathbf{P}}^{\mathbf{NL}}, \tag{14}$$

where ϵ_r is the frequency dependent relative permittivity of the medium, and insert the following expression into eq. (13):

$$-\nabla^2 \tilde{\mathbf{E}} = \frac{\epsilon_r(\omega)}{c^2} \frac{d^2 \tilde{\mathbf{E}}}{dt^2} + \frac{1}{\epsilon_0 c^2} \frac{d^2 \tilde{\mathbf{P}}^{\mathbf{NL}}}{dt^2}, \tag{15}$$

which is our nonlinear wave equation.

2.2.2 Intensity of the second harmonic

The nonlinear wave equation, eq. (15), can be expanded into components of different frequencies, or rather the electric field $\tilde{\mathbf{E}}$ along with the nonlinear polarization field $\tilde{\mathbf{P}}^{\mathbf{NL}}$ can be expressed as [4]

$$\tilde{\mathbf{E}} = \sum_n \tilde{\mathbf{E}}_\mathbf{n}(\mathbf{r}, t) \tag{16}$$

$$\tilde{\mathbf{P}}^{\mathbf{NL}} = \sum_n \tilde{\mathbf{P}}^{\mathbf{NL}}_\mathbf{n}(\mathbf{r}, t), \tag{17}$$

where *c.c.* is the complex conjugate of the preceding term. Each component of the $\tilde{\mathbf{E}}$ and $\tilde{\mathbf{P}}^{\mathbf{NL}}$ can be represented as the complex amplitudes

$$\tilde{\mathbf{E}}_\mathbf{n} = \mathbf{E}_\mathbf{n} e^{-i\omega_n t} + c.c., \tag{18}$$

$$\tilde{\mathbf{P}}^{\mathbf{NL}}_\mathbf{n} = \mathbf{P}^{\mathbf{NL}}_\mathbf{n} e^{-i\omega_n t} + c.c. \tag{19}$$

Using eq. (16) and eq. (17) the wave equation (15) can be rewritten for a specific frequency component as

$$-\nabla^2 \tilde{\mathbf{E}_\mathbf{n}} = \frac{\epsilon_r(\omega)}{c^2} \frac{d^2 \tilde{\mathbf{E}_\mathbf{n}}}{dt^2} + \frac{1}{\epsilon_0 c^2} \frac{d^2 \tilde{\mathbf{P}}^{\mathbf{NL}}_\mathbf{n}}{dt^2}. \tag{20}$$

The wave equation is now valid for n components, we are interested in the SH and denote the sum frequency component as $\tilde{\mathbf{E}}_\mathbf{3}$, which is the product of the components $\tilde{\mathbf{E}}_\mathbf{1}$ and $\tilde{\mathbf{E}}_\mathbf{2}$. We conclude that with a small contribution from the nonlinear polarization the solution of eq. (20) for a wave propagating on the z direction will still be in the form of

$$\vec{E}_3(z, t) = A_3 e^{k_3 z - \omega_3 t} + c.c.. \tag{21}$$

The nonlinear polarization is

$$\tilde{\mathbf{P}}^{\mathbf{NL}}_\mathbf{3} = \mathbf{P}^{\mathbf{NL}}_\mathbf{3} e^{-i\omega_3 t}, \tag{22}$$

where $\mathbf{P}^{\mathbf{NL}}_\mathbf{3}$ can be rewritten using eq. (4) as

$$\mathbf{P}^{\mathbf{NL}}_\mathbf{3} = 4\epsilon_0 d \mathbf{E}_\mathbf{1} \mathbf{E}_\mathbf{2}. \tag{23}$$

Using eqs. (21), (22), (23) and inserting them into the wave equation (20) we can differentiate with respect to time and space. ∇^2 can be replaced with $\frac{d^2}{dz^2}$ since we only have defined a

field in the z-axis. The expression obtained is thus

$$\left[\frac{d^2A_3}{dz^2} + 2ik_3\frac{dA_3}{dz} - k_3^2A_3 + \frac{\epsilon_r(\omega_3)\omega_3^2}{c^2}A_3\right]e^{-i(k_3z-\omega_3t)} + c.c. \tag{24}$$
$$= -\frac{4\epsilon_0 dA_1A_2\omega_3^2}{\epsilon_0 c^2}e^{-i((k_1+k_2)z-\omega_3t)} + c.c.$$

Where A_1 and A_2 are the amplitudes of the two waves producing the second harmonic. They are defined in a similar fashion as seen in eq. (21). The complex conjugates in eq. (24) can be dropped without introducing an inequality [4]. Furthermore the third and fourth term can be rewritten using

$$k_3 = \frac{n_3\omega_3}{c}, \qquad \epsilon_r(\omega_3) = n_3^2 \tag{25}$$

so it becomes apparent that they are equal and thus cancel each other. The first term of eq. 24 can be assumed negligible due to the slowly varying envelope approximation [5] and ultimately the exponential frequency term can be removed from both sides. Rearranging the exponential phase terms to the same side yields following simplification of eq. 24:

$$2ik_3\frac{dA_3}{dz} = -\frac{4dA_1A_2\omega_3^2}{c^2}e^{i(k_1+k_2-k_3)z}, \tag{26}$$

and the quantity

$$\Delta k = k_1 + k_2 - k_3 \tag{27}$$

is assigned, where Δk is called the phase mismatch. To ease calculation we assume that A_1 and A_2 are not dependent on z and thereafter integrate eq. (26) over the length of the medium L in order to obtain an expression for the amplitude of the second harmonic.

$$A_3 = \frac{2idA_1A_2\omega_3^2}{k_3c^2}\int_0^L e^{i\Delta kz}dz = \frac{2idA_1A_2\omega_3^2}{k_3c^2}\left(\frac{e^{i\Delta kL}-1}{i\Delta k}\right). \tag{28}$$

The intensity is proportional to the square of the amplitude. Besides, from the amplitudes of the fundamental waves it is also proportional to the phase difference Δk as follows:

$$I_3 \propto \left(\frac{e^{i\Delta kL}-1}{i\Delta k}\right)^2 = \frac{2-2\cos\Delta kL}{\Delta k^2} = 4L^2\frac{\sin^2\Delta kL}{(\Delta kL)^2} = L^2\mathrm{sinc}^2\Delta k/2 \tag{29}$$

3 Design

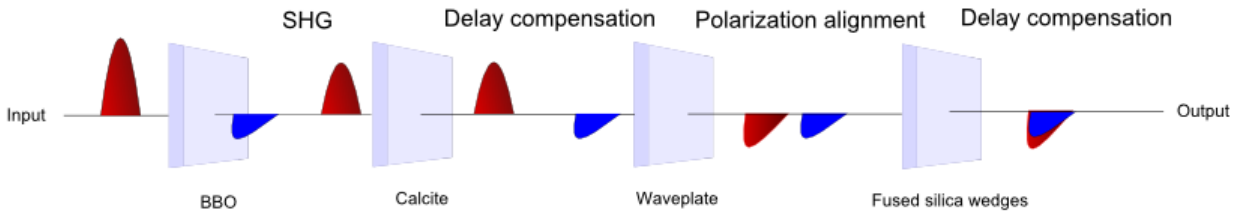

Figure 1: A schematic presentation of the assembly. The materials that are labelled in the figure are of course specific for the desired wavelength, both in dimensions and material type. Not included in the figure are polarisers for cleaning ellipticity, which normally is important. An explanation for the "two-stage" delay compensation is provided in **Sec.3.3**

The collinear design implies that both colors co-propagate in the interferometer. This means that materials have to be chosen with respect to both the 1300nm and 650nm pulse. Seen in Fig. 1 are the essential components for the setup. The input is a 300nm broad pulse centred at 1300nm, the first material that it is transmitted through is a BBO crystal with a cut axis for best possible phase matching for frequency doubling of this wavelength. As it is transmitted through the BBO crystal it will produce a second harmonic that propagates together with the fundamental beam, although oscillating orthogonally to it and being slightly delayed in time (appearing exaggerated Fig. 1). The calcite crystal is used to control the delay between the two pulses. As Calcite is highly birefrigent, *i.e.*, there is a large difference in the refractive indices of the fast and the slow axis of propagation, it can be placed in such a manner that the shorter wavelengths travel faster than the longer wavelengths. Preferably it should overcompensate at this stage, since both pulses have more material to travel through, and most materials have normal dispersion; "red" is faster, "blue" is slower (where red and blue imply, short and long wavelength respectively). The placement of the calcite delay plate is important, it must precede the waveplate since the pulse is very linearly polarized before its polarization is rotated, as opposed where it is slightly elliptical after the waveplate. It is also at this stage that the two field components are orthogonal and can be delayed separately. The light enters the waveplate at an angle. The waveplate, being birefringent, delays the phase of the projections on the fast and slow axis of the pulse as it propagates through it, and as such it "rotates" its state of polarization. The waveplate is designed so that it rotates the fundamental pulse by a quarter of a revolution and the SH by half a revolution, effectively aligning the polarization of the pulses parallel. During the passage a small amount of ellipticity may be introduced, which if too large has to be filtered by polarisers. The last component pictured in Fig. 1 are two fused silica wedges (although it is drawn as a single rectangle) that provide a possibility of fine tuning the delay between the pulses. Fused silica

is not birefringent and can therefore be placed after the waveplate.

3.1 Phase matching

A good starting point in order to determine a suitable crystal for frequency doubling is to find a material with a large second order susceptibility d. The SHG depends strongly on the phase mismatch as seen in eq. (29), meaning that it is important to have good phase matching. The phase matching condition is given by:

$$k_1 + k_2 = k_3, \tag{30}$$

which can be rewritten as:

$$\omega_1 n_o(\omega) + \omega_2 n_o(\omega) = \omega_3 n_e(\omega, \theta). \tag{31}$$

Since the input light is linearly polarized, the two waves that mix will be of the same type of rays (ordinary or extraordinary), a form of self interaction, whose mixing will result in a ray with orthogonal polarization. This is called ooe mixing or Type 1 mixing.
Since the pulse is not monochromatic one must consider the three wave mixing to result from many possible combinations of the different wavelengths in the bandwidth. A way to perform this is to use MatLab and combine all possible outcomes of mixing. First the refractive indices for all the wavelengths are calculated. Then calculate the phase matching in accordance with eq. (31). In MatLab one can also rotate the crystal axis in order to see which incoming angle provides best phase match. It is possible to express the refractive index as a function of the cut angle with:

$$\frac{1}{n(\omega, \theta)^2} = \frac{\sin^2 \theta}{n_o(\omega)^2} + \frac{\cos^2 \theta}{n_e(\omega)^2}, \tag{32}$$

where n_e and n_o are the refractive indices of the extraordinary and ordinary refractive indices of the crystal. The refractive indices can be calculated using Sellmeier equation which for a non specified material is

$$n(\lambda) = \sqrt{1 + \sum_j \frac{A_j \lambda^2}{\lambda^2 - B_j}}, \tag{33}$$

where A_j and B_j are constants that are experimentally determined for a material. The data for different materials were retrieved from *refractiveindex.info* [6] in order to make the calculations in this report.
The tuning curve is produced by calculating the phase mismatch for a certain wavelength according to eq. (12), and extracting for which angle this phase mismatch is as small as

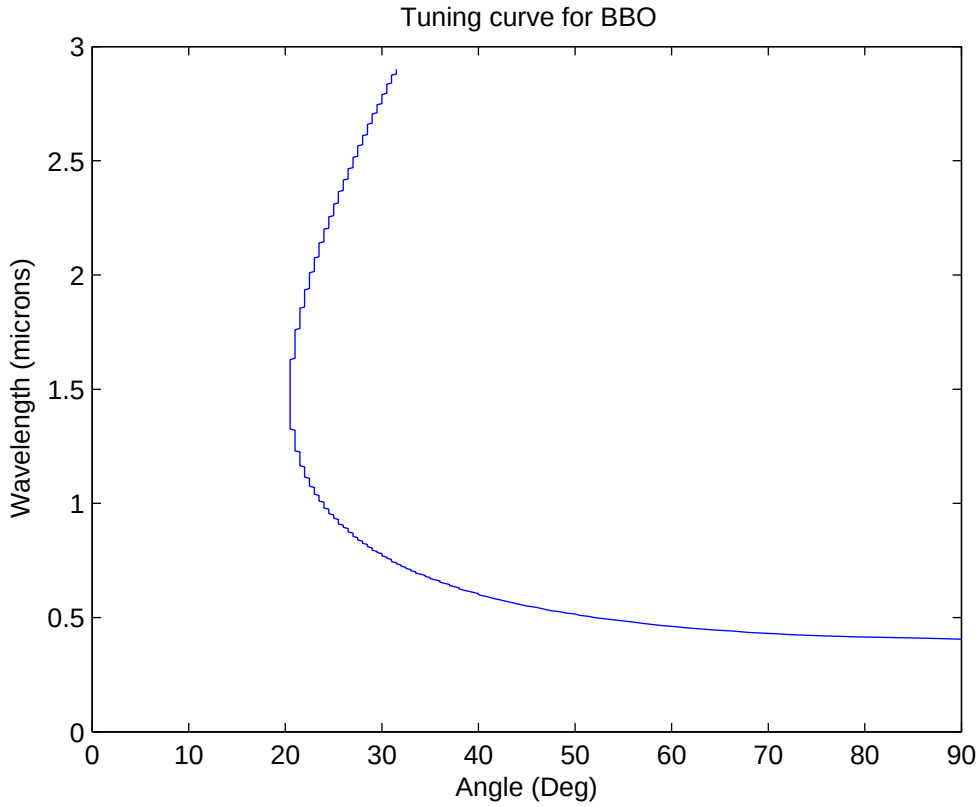

Figure 2: The tuning curve for BBO

possible. The tuning curve provides a good overview regarding the behavior of the crystal. For instance seen in Fig.2. it is clear that the wavelength 1300nm and a decent bandwidth would be well fulfilled, due to the steep shape of the line in the plot. The tuning curves provide an indication of the best cut angle for phase matching in a crystal. The optimal cut angle calculated for 1300nm±150nm in a BBO crystal is 20.93°. BBO is chosen mainly since it has a large optical transparency, large nonlinear coefficient and is highly birefringent. When the crystal cut angle is determined, the dimensions of the crystal must be determined. In order to have an upper limit on the crystal thickness one can use the wave mixing coherence length formula (using eq. 27 & 29):

$$L_c \cdot |\Delta k| \leq \frac{\pi}{2} \tag{34}$$

where L_c, known as the coherence length, is the largest length for a given phase mismatch in order to have efficient wave mixing. The value of the coherence length will set the upper limit of the crystals length. The coherence length calculated was 1.09mm. A BBO of length 0.3mm that was in stock was ultimately used in the design.

3.2 Polarization alignment

3.2.1 General principle

The second harmonic will be orthogonally polarized to the incoming light, meaning that unless rotated it will remain so when transmitted through the interferometer. Both of the waves have to be rotated so that they have the same direction of polarization. This can be done by using a medium that acts as a half-wave plate for one of the waves and as a full-wave plate for the other. The rotation per unit length is given by [7]:

$$\frac{\beta}{d} = \frac{\pi}{d\lambda}(n_e - n_o) \tag{35}$$

which is denoted as the specific rotary power. β is the angle of rotation that the polarization makes for a given wavelength λ, which is analogous with a phase delay between the two spatial components of the oscillating light. d is the distance traversed in a medium with a given β. If the material is very birefringent, the light will make revolutions even when transmitted through a thin piece of the medium. For instance, coming in at an angle 30° from the ordinary axis into a 1mm thick piece of calcite, the light centred at 1300nm will have rotated more than 10 times before it exits. For the broadband pulse this will also mean that one side of the broadband spectrum rotates two full revolutions more than the other, which produces a lot of ellipticity. In the setup, only the waveplate will rotate the light, all the other components will transmit the light along one of their axes. When the light has been rotated to the correct state of polarization the pulse will almost inevitable be elliptical. To calculate the amount of ellipticity introduced by the designed interferometer one can use ray transfer matrices, also called Jones matrices

$$\begin{bmatrix} x' \\ y' \end{bmatrix} = M_n \cdot M_{n-1} \cdot M_{n-2} \cdot ... \cdot M_2 \cdot M_1 \cdot \begin{bmatrix} x \\ y \end{bmatrix} \tag{36}$$

where, x and y provide the state of polarization of the light prior to the waveplate and x' and y' is the polarization state after transmission through the waveplate. The M_n terms represent the matrices of the material. For the sake of calculating the ellipticity, the media will be treated as a wave plate when using the ray transfer matrices. The matrix for a wave plate is given by:

$$\frac{1}{\sqrt{2}} \begin{bmatrix} e^{i\beta} & 0 \\ 0 & e^{-i\beta} \end{bmatrix} \tag{37}$$

where β is the phase delay, the same one as given in eq. (34). When the light passes through the system, the polarization will rotate if the material is birefringent and the polarization

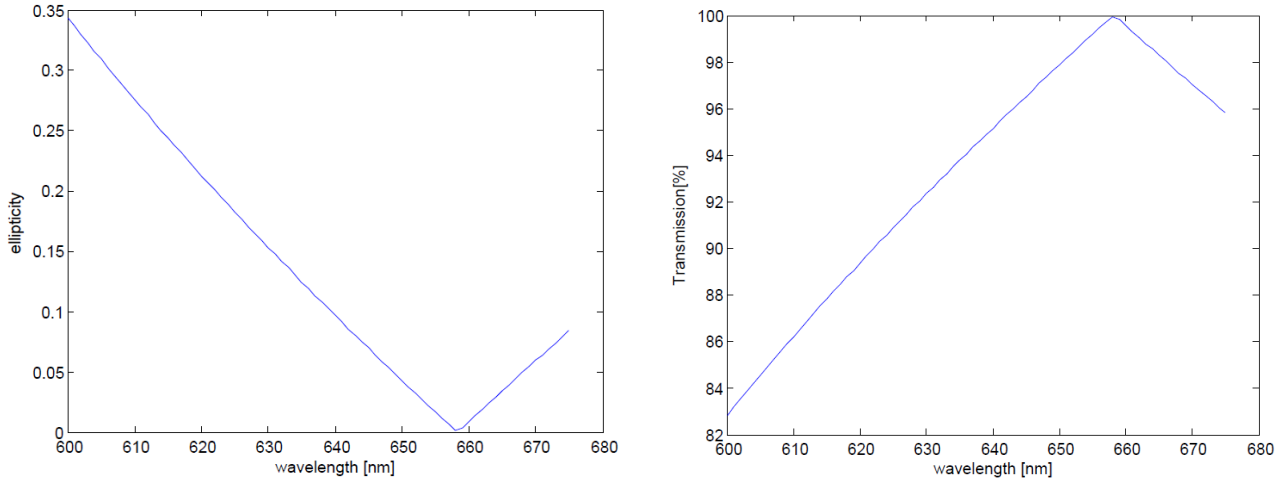

(a) 650nm pulse ellipticity. **(b)** 650nm transmission.

Figure 3: The ellipticity of the 650nm pulse when it passes 73μm quartz. If all unwanted polarization is cleaned afterwards, then the pulse would had been transmitted according to the right panel.

state of the field is not aligned along the ordinary or extraordinary axis, this information will be contained on the left side of eq. (35). The values of x' and y' are complex quantities. To calculate the ellipticity one can use:

$$\sin^2 2\chi = \frac{2R}{1+R^2}\sin\phi, \tag{38}$$

where R is the ratio between the magnitudes of the x' and y' and ϕ is the phase difference between the waves. χ is the angle between the orthogonal components of the elliptically polarized light, hence the arctangent of χ is a measure of the ellipticity.

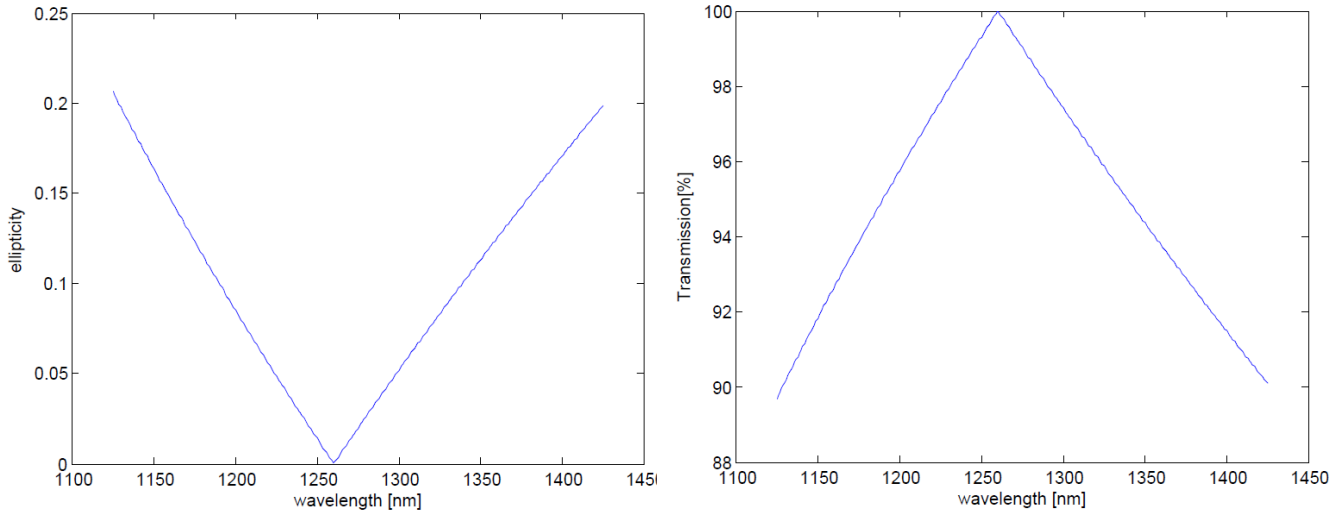

(a) 1300nm pulse ellipticity.

(b) 1300nm transmission.

Figure 4: Same set of pictures as in Fig. 3 but with the central frequency of the pulse being 1260nm.

Figures 3 and 4 represent the ellipticity introduced when the fundamental wave passes through quartz with thickness to rotate it a quarter of a revolution and simultaneously rotate the second harmonic a half revolution (conventionally referred to as a λ-half and a λ plate respectively). Since both the pulses are not monochromatic, the different wavelengths of the pulses are rotated differently. This leads to the quartz acting as an "almost" λ-half and λ waveplate for some regions of the pulses. As it appears from figures 3 and 4 the transmission does not undergo a dramatic loss. The polarization may then be cleaned of its ellipticity before the pulses are transmitted to be used for HHG. However that would require quite some Brewster windows, which themselves add to dispersion. For instance, to reduce the ellipticity of the upper and lower endpoints of the wavelength spectrum in figure 4a to 0.05 would require 8 plates of BK7 glass at Brewster angle. The plates induce additional dispersion which could be problematic. Elliptic polarization of the light reduces the efficiency of the HHG. An ellipticity of 0.2 (as is the case of Fig. 4a) would halve the signal strength of the 17th harmonic order, and consecutively weaken the higher orders for 800nm [8]. The effect is less destructive for 1300nm as the signal strength reduction scales with the inverse of the wavelength[9]. Quartz was not the only material tested for a waveplate; calcite, sapphire, BBO and MgF2 (magnesium fluoride)were also calculated, but quartz introduced the least ellipticity. This means that it is inadequate to use conventional birefringent crystals given our desired ellipticity tolerance and another solution is required to overcome this problem.

3.2.2 Achromatic dual wave plate

A custom wave plate was produced by the company *Bernard Halle Nachfolger GmbH* that introduced minimal ellipticity by simulatenously acting as an achromatic half-waveplate for 650 nm and an achromatic fullwaveplate for 1300 nm. The crystal is thus an achromatic dual wave plate. Note that the SH is rotated more than the fundamental, and that the final state of the polarization for both waves is orthogonal to that of the incoming light. The wave plate consists of three different birefringent crystals. Two rather "thick" crystals which are placed with crossed optical axes and a thin zero order waveplate between them at an specific angle. All of them placed together to form a dual wave achromatic plate.

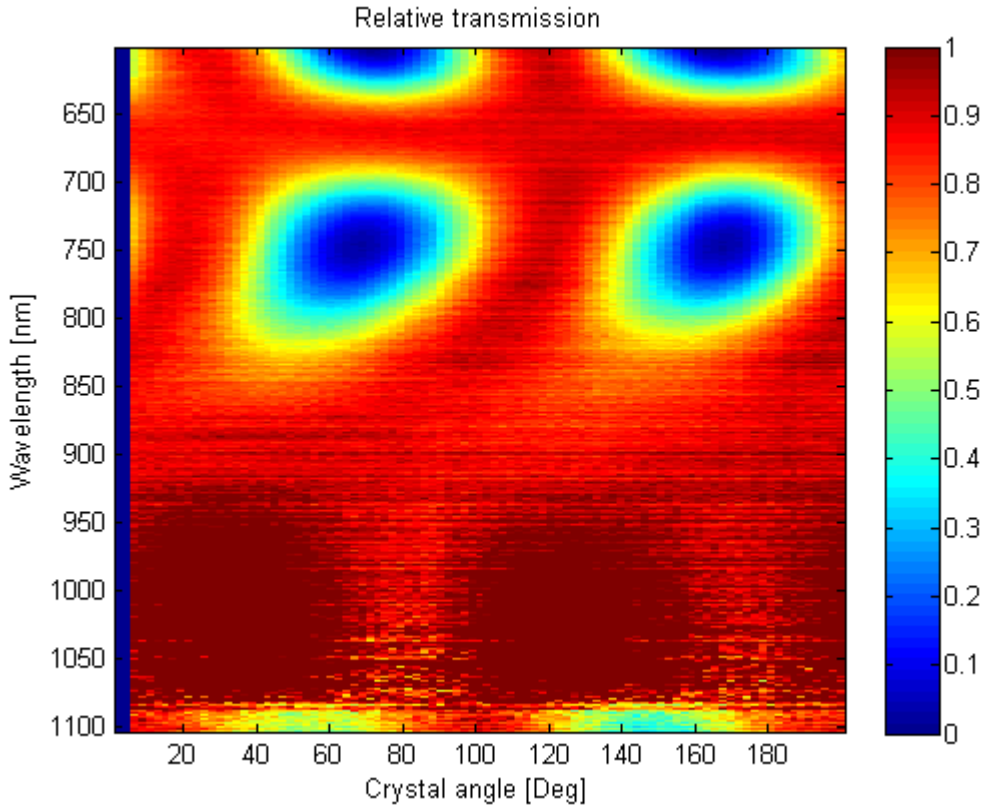

Figure 5: Transmission of polarized light through the achromatic dual wave plate for the SH. The plate is placed between two parallel plane polarisers and then rotated.

The dual wave plate was tested using a simple experimental setup. Two parallel plane polarisers were placed with the wave plate between them. An incandescent lamp was used as a white light source, and the transmission through the polarisers and the wave plate was measured. In figure 5 we see the spectrum of the white light source as it has passed the setup. The figure consists of 90 spectra of the white light source that are rotated 2° in each step; each of the readings are normalised with a spectrum where only the polarisers are between the white light source and the detector. The figure shows that the wave plate works as a full wave-plate

for 650 nm at any angle, in some regions the crystal works as a full wave-plate for a broad part of the spectrum, for instance near 120°. The project of measuring the entire intended spectrum and the dispersion for the achromatic dual wave plate is planned to be performed in the future, as it is of high interest for both the *Department of Atomic Physics* in Lund and *Bernard Halle Nachfolger GmbH.*

3.3 Delay compensation

Since the materials are dispersive they will displace the two pulses of different color in time with respect to each other. This is the same effect that makes the pulse broader, but the central frequencies are more spaced in frequency than the endpoints of the frequency broadbands, hence generating a greater temporal displacement. Since the propagation of the pulses is the group velocity it is possible to derive the difference in time it takes for two pulses to traverse through the material of length L:

$$\tau_1 = \frac{L}{v_{g1}} \qquad \tau_2 = \frac{L}{v_{g2}} \tag{39}$$

$$\tau_{GVM} = \tau_1 - \tau_2 = \left(\frac{L}{v_{g1}} - \frac{L}{v_{g2}}\right) \tag{40}$$

where τ_1 and τ_2 denote the time for the pulses to travel through the material. τ_{GVM} is the difference of the times, the delay between the two pulses. v_g is the group velocity, which is given by:

$$v_g = \frac{c}{n - \lambda_0 \frac{dn}{d\lambda_0}} \tag{41}$$

for light with wavelength λ_0 through a material with refractive index n. Hence v_{g1} and v_{g2} in eq. (40) are the group velocities for the different pulses as they propagate through a material with length L. It is possible to calculate these velocities by using the aforementioned Sellmeier equations (see **Sec.3.1**).

Calcite was chosen as a delay plate, since calcite is very birefringent. As demonstrated in Fig. 6, the group velocity is faster in the fast axis than in the slow for any given wavelength in the regime for which the setup is designed for. The speed difference of light the ordinary and extraordinary axis in calcite is much larger than in any other components, meaning that the temporal tuning with calcite is very effective. Besides from reducing the delay between the pulses, a method to control the delay was desired. Originally the option of having two calcite wedges with crossed axis proved to be optimal when it comes to having a large range of tuning, but proved to be problematic since the beam is quite large, and using such wedges

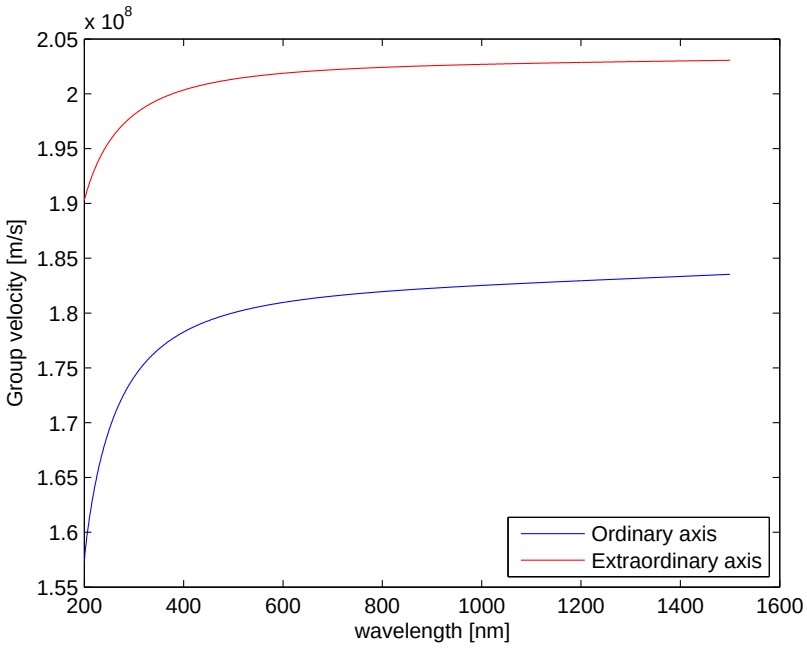

Figure 6: The group velocity for light of different wavelengths when traveling through calcite.

Material	**BBO**	**FS**	**Waveplate**	**air**
Thickness [mm]	0.3	4.33	2	1000
$\tau_{\mathbf{GVM}}$ **[fs]**	-71.64	138.8	62.8	9.31
Total $\tau_{\mathbf{GVM}}$ **[fs]**	139.27			

Table 1: Group delay between the pulses introduced by the components. In this particular table calcite is excluded, since it is determined by the delay from the other components.

would result in parts of the beams projection having different thick paths of ordinary and extraordinary calcite to cross. This is undesired since it would induce spatial deformation of the pulses. Another option was to have wedges of calcite with parallel axes, but such wedges have to be very thin because of the high birefringence of calcite,thereby brittle, and also costly. Ultimately the solution of having a regular plate of calcite proved to be most efficient, durable, and cost efficient solution, and the tuning would be provided from fused silica wedges. A calculation could then be performed for what the thickness of the calcite plate would be, provided that all other materials were accounted for.

In Table.1 a list of the components and the corresponding delays they introduce is provided. The calcite crystal was chosen to slightly overcompensate the total delay despite the fact that all delays are accounted for. The reason for this is that it is easier to add more glass as opposed to ordering another calcite crystal, given the scenario that it undercompensates the delay.

Seen in Fig.7 it is possible to have a close to zero temporal offset of the central frequencies

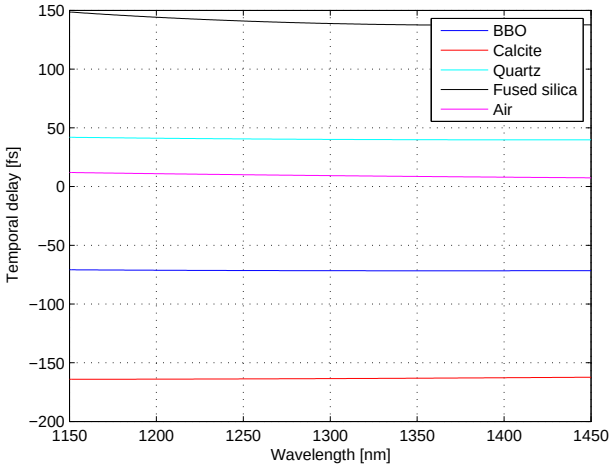

(a) The delays between a 1300nm pulse and a 650nm pulse. The components are of the thickness that is intended to be used for delay compensation.

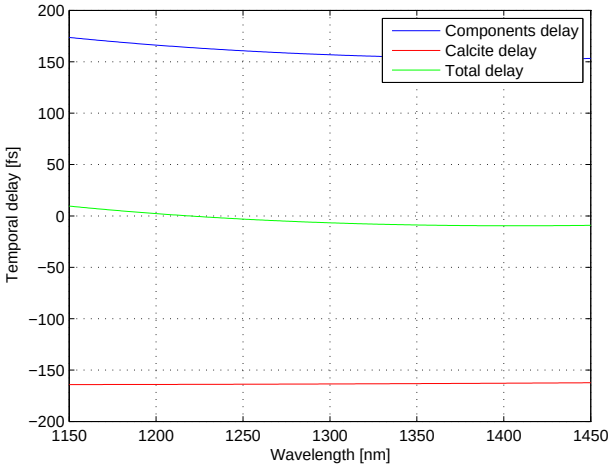

(b) Time delays between a 1300nm pulse and a 650nm pulse where all but calcite is fused as "components".

Figure 7: The delay introduced by the components is plotted in matlab. The plot is done not only the central frequency, but a span of wavelengths close to the central frequency intended to be used. In the right figure, the components are added together and the thickness of the calcite can be changed in order for the total delay to be as small as possible.

of the pulses. The wavelength regime rendered in the plots is purely esthetic since the delays of the central frequencies are of the essence. Given that most compenents inherit an error in dimensions when they are manufactured the tuning device becomes important to reduce the delay between the pulses. The wedged fused silica pieces provide approximately 4mm range tunability. This in turn corresponds to 130fs in terms of delay. The wedges are connected to a translation stage for increased precision.

3.4 Dispersion

The components in the construction will disperse the light (much like any medium tends to). The dispersion will result in a delay in time for the different pulses, but also a stretching of the pulse duration. Two effects will have to be corrected before transmitting the light. Group delay dispersion (GDD) is the phenomenon of the phase stretching due to dispersion. The group delay dispersion is mathematically the derivate of the phase with respect to the angular frequency, but it can be rewritten in the form of:

$$GDD = \frac{\lambda_0^3}{2\pi c^2}\frac{d^2}{d\lambda_0^2}n = \beta' \tag{42}$$

i.e. as the second derivative of the Sellmeier equations for a medium with respect to the central wavelength of the pulse (normally given in the scale of fs^2). Additionally there is

"third" order dispersion of the medium (TOD $[fs^3]$), which is the third derivative of the phase with respect to the angular frequency, or as implemented in the code used as:

$$TOD = \frac{d}{d\omega}\beta' = -\frac{\lambda_0^2}{2\pi c_0}\frac{d}{d\lambda_0}\beta' = \beta'' \tag{43}$$

and yet, a fourth order dispersion is also calculated (FOD $[fs^4]$) in the very similar fashion as above [10]. Higher order dispersions are assumed to be low compared to the four first dispersions. In order to correct the dispersion it is preferable to introduce dispersive media which have opposite dispersive properties than due to the ones used to make the device function, for instance calcite plates.

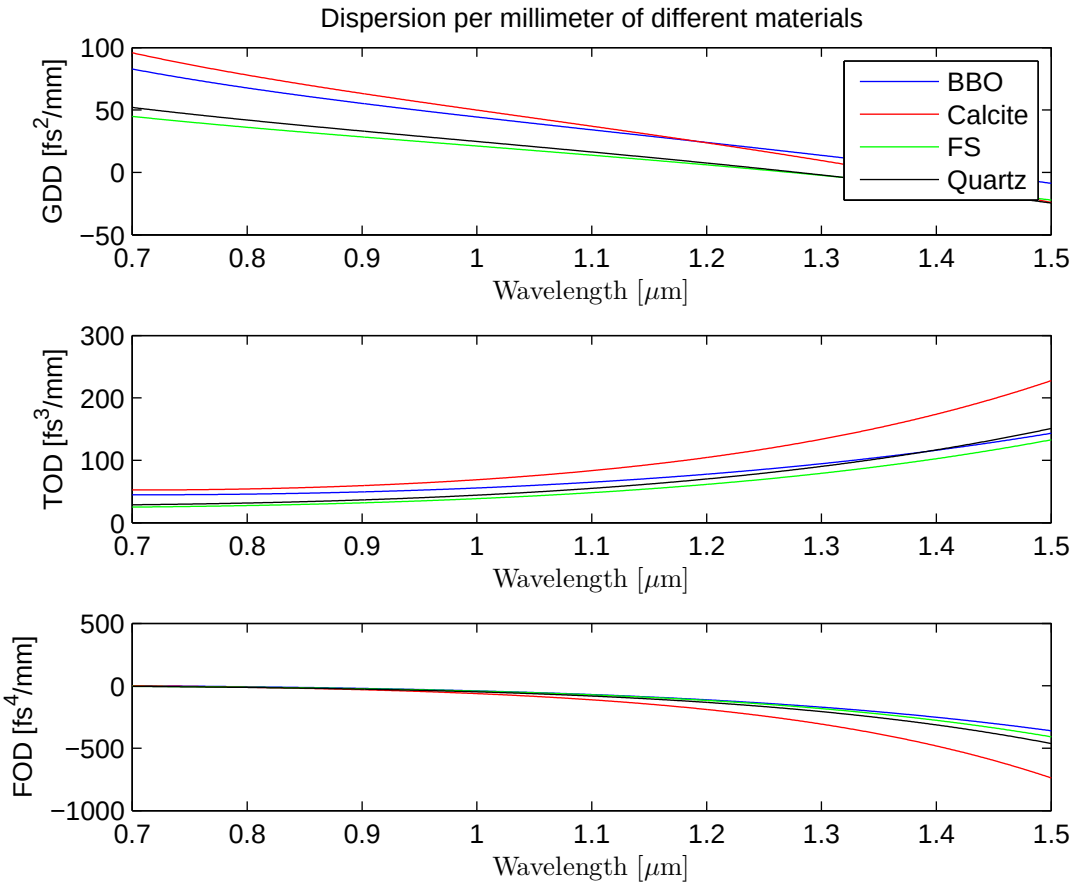

Figure 8: Dispersion introduced from the materials in the interferometer

Material	**BBO**	**Calcite**	**FS**
Thickness [mm]	0.3	0.32	4
GDD 1300nm [fs^2]	7.0520	-21.6090	-21.7324
GDD 650nm [fs^2]	46.6692	68.7822	402.1321
Broadening 1300nm	1.0000	1.0002	1.0017
Broadening 650nm	1.0009	1.0019	1.0618
Total broadening 1300nm	1.0026		
Total broadening 650nm	1.1004		

Table 2: The broadening of the pulse when traversing through the setup.

In figure 8 the dispersions introduced by the components as a function of wavelength are presented. Note that there are 15 orders of magnitude that separates one order of dispersion from a consecutive higher one. To reduce the dispersion a material with an opposite sign of dispersion is usually placed in the beam trajectory. Unfortunately such materials do not exist for the near infrared region [11], let alone for the visible region (where the SH is centred), as most of the dispersions change sign near 1.2-1.3μm. In the moment of writing there is no greater need for reducing the dispersion, neither was an appropriate solution found. The main issue is that no material was found to reduce the dispersion for both waves simultaneously (calcite has opposite sign of dispersion near the 1300nm regime, but not for the second harmonic of that regime). The dispersion does not seem to be too large.
One can calculate the influence of the dispersion on the pulses. The easiest and most intuitive way is to look at the pulse broadening through the components, although this is just "half" the story since only the GDD is taken into consideration, it does pose the main issue. The pulse broadening is given by[12]:

$$\tau = \tau_0 \sqrt{1 + \frac{{D_2}^2}{{\tau_0}^4}} \tag{44}$$

where τ is the pulse duration after transmission of a beam with duration τ_0 through a material with GDD D_2.
The pulse duration used in table 2 was 40**fs**. The broadening of the fundamental pulse is 0.26% and the broadening of the SH is 10%. The broadening will become larger if the pulse duration is shortened, but 40**fs** is assumed to be short enough.

4 Outlook

The collinear setup has to be tested with the pulses that it is designed for. The most relevant way of testing it is to infact generate high-order harmonics, because in the end that is what it is designed for. Possible impediments for the functionality of the interferometer is the ellipticity of the light after passing the waveplate not being low enough and the pulse delay not being compensateable with before mentioned materials. Both issues can be solved. The ellipticity can be filtered using brewster windows and the delay can be tuned by adding more glass. The delay is overcompensated as it is by the calcite crystal and even in the event of the ellipticity being small enough one could additionally reduce it by recplacing the glass with brewster windows.

References

[1] P.M. Paul et al., *Observation of a Train of Attosecond Pulses from High Harmonic Generation*. SCIENCE 1 June, 2001.

[2] P.B. Corkum., *Plasma perspective on strong-field multiphoton ionization*. PHYSICAL REVIEW Volume 71, 1993.

[3] B.E.A. Saleh, *Fundamentals of photonics*. 2nd Edition, 2007.

[4] Robert W. Boyd, *Nonlinear Optics*. 3d Edition, p.73-75, 2008.

[5] Peter W. Milonni, J. H. Eberly, *Lasers*. p.250, 1988.

[6] `http://refractiveindex.info/`

[7] `http://scienceworld.wolfram.com/physics/SpecificRotaryPower.html`

[8] V.V.Strelkov, *Theory of high-order harmonic generation and attosecond pulse emission by a low-frequency elliptically polarized laser field*. PHYSICAL REVIEW A 74, 2006.

[9] Max Möller et al., *Dependence of high-order-harmonic-generation yield on driving laser ellipticity*. PHYSICAL REVIEW A 86, 2012.

[10] `http://ticc.mines.edu/csm/wiki/images/f/f0/UFO05-Dispersion.pdf`

[11] Miranda, M. (2012). *Sources and Diagnostics for Attosecond Science*. Ph.D. Thesis. Lund University: Sweden.

[12] `http://www.rp-photonics.com/chromatic_dispersion.html`